Asociación Argentina
de Mecánica Computacional

Mecánica Computacional Vol XXXIX, págs. 39-48 (artículo completo)
F.E. Dotti, M. Febbo, S.P. Machado, M. Saravia, M.A. Storti (Eds.)
Bahía Blanca, 1-4 Noviembre 2022

PITFALLS IN THE USE OF DISCRETE MODELS WITH CUTTING DYNAMICS FOR DRILL-STRINGS

Hector E. Goicoechea[a,b], Roberta Lima[a], Fernando S. Buezas[b] and Rubens Sampaio[a]

[a]*Laboratório de Vibrações, Pontifícia Universidade Católica do Rio de Janeiro (PUC-Rio), Rua Marquês de São Vicente 255, Gávea,Rio de Janeiro, 22451-900, Rio de Janeiro, Brasil*

[b]*Instituto de Física del Sur (IFISUR), Departamento de Física, Universidad Nacional del Sur, CONICET, Av. L. N. Alem 1253, Bahía Blanca, B8000CPB, Buenos Aires, Argentina*

Keywords: Drill-string dynamics, cutting dynamics, drill-string models

Abstract. In this paper, an established 2 degrees-of-freedom drill-string model (one axial, one torsional) is compared against another model consisting of 1-axial-DOF and a continuous torsional formulation. Some application cases considering different operation conditions for a 1200m drill-column are simulated. The results show that the dynamics can differ considerably. This suggests that the 2-DOF approach may be capuring aspects of the dynamics that are neglected in the 2-DOF approach.

1 INTRODUCTION

Rotary drilling systems (drill-strings) are essential tools used in the extraction of oil and gas. They are mainly composed of a set of tubes that are responsible for transmitting the forces and torques from the top of a well to the bit, at the bottom. It is known that drill-strings are very slender structures that may undergo complex dynamics: they may exhibit oscillations and stick-slip (Brett (1992); Lima and Sampaio (2015); Saldivar et al. (2016)), buckling and other phenomena such as failure due to fatigue (Vaisberg et al. (2002); Macdonald and Bjune (2007)).

Up to the authors' knowledge, there is no clear consensus on what type of model better captures the dynamics of these slender structures. To name a few papers that intend to capture the dynamics of real-scale structures using lumped formulations, Richard et al. (2007) present a 2-DOF model to study the cause of drill-string stick-slip vibrations, considering a theoretical blunt polycrystalline diamond compact (PDC) cutter; and Tian and Detournay (2021) use a 2-DOF approach to construct a stability map, extending the bit-rock interaction model of Richard et al. (2007) to account for a realistic cutter layout.

In contrast, continuous descriptions are found in Trindade et al. (2005); Sampaio et al. (2007), in which continuous bar and shaft formulations are used to obtain the dynamics of a drill-string; Piovan and Sampaio (2009) uses a geometrically non-linear model based on the Bernoulli-Euler hypothesis, capable of simulating the axial, torsional and flexural dynamics; Goicoechea et al. (2019) takes a continuous formulation based on the Cosserat theory of rods to study the dynamics of an off-bottom drill-string in a curved bore-hole; and Aarsnes and van de Wouw (2019) employs a distributed axial-torsional approach. The authors of the latter show "how multiple axial modes are excited or attenuated, depending on the bit rotation rate", and therefore it is suggested that "a lumped drill-string approximation is insufficient for the general case", with regard to the behaviour observed in the axial dynamics.

The motivation for concentrated formulations is usually related to integration times, simplicity, or the capacity to tackle the problem analytically, which is often more difficult when continuous formulations are employed. Deciphering whether a continuous or a discrete approach should be used to capture the dynamics of drill-strings is not evident. The objective of this work is to show that to use a 1- or 2-DOF model to simulate the dynamics of a real scale drill-string may be an oversimplification of the problem that could lead to innacturate results. This study represents a first step to assess the suitability of the different approaches, where the bit-rock interaction forces are the only responsible for the dissipative terms considered.

2 THE DRILL-STRING MODELS

In this study, two different structural models are employed to simulate the dynamics of the drill-string (Fig. 1), namely M1 and M2. A modification of the 2-DOF approach employed in Richard et al. (2007) is used in model M1: 1-DOF is used to account for the torsional dynamics, and 1-DOF for the axial one. In model M2 the torsional dynamics are tackled with a continuous formulation, while retaining the 1-DOF approach for the axial motion.

2.1 The axial dynamics model

Naming U the position of the bit, W_0 the difference between the submerged weight and the hook load and W a reaction force due to the bit-rock interaction, the axial dynamics for M1 and M2 is described by

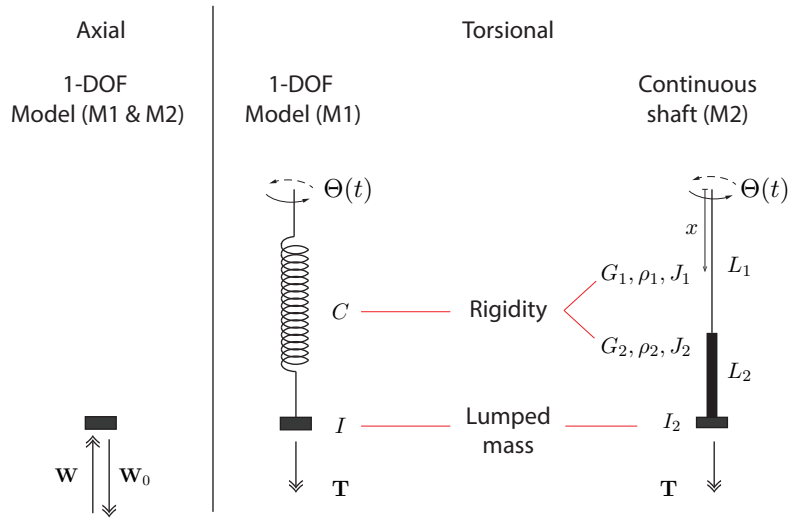

Figure 1: A sketch showing the two models employed, M1 and M2. Model M1: M is a mass, I an inertia, C a spring constant. Model M2: two different cross-sections are considered with J_1, J_2 being the geometric moment of inertia of the drill-pipes and the bottom hole assembly (BHA), respectively; G_1, G_2 the shear elastic moduli; and ρ_1, ρ_2 the densities of the material. At the lower end, a concentrated inertia I_2 is considered.

$$M\frac{d^2U}{dt^2} = W - W_0 \tag{1}$$

2.2 Torsional dynamics - Model M1

Calling Φ the angular displacement of the bit, C a spring constant to account for the rigidity of the drill-pipes, I the concentrated inertia to account for the bottom hole assembly (BHA) and T the torque-on-bit due to the bit-rock interaction, the torsional dynamics in model M1, like in Richard et al. (2007), are given by

$$I\frac{d^2\Phi}{dt^2} + C(\Phi - \Theta) = T \tag{2}$$

2.3 Torsional dynamics - Model M2

The behaviour of the drill-string is modelled by means of a continuum in model M2. Considering the domains $x_1 \in [0, L_1]$, and $x_2 \in [L_1, L_1 + L_2]$, and a parameter $\alpha \in [0; 1]$, the problem is described by

$$G_j J_j \frac{\partial^2 \Phi_j}{\partial x_j^2} = \alpha \rho_j J_j \frac{\partial^2 \Phi_j}{\partial t^2}, \text{ with } j = \{1, 2\}, \text{ and} \tag{3}$$

$$\Phi_1(x = 0, t) = -\Theta(t), \quad \Phi_1(x = L_1, t) = \Phi_2(x = L_1, t)$$

$$G_1 J_1 \frac{\partial \Phi_1}{\partial x_1}(x_1 = L_1, t) = G_2 J_2 \frac{\partial \Phi_2}{\partial x_2}(x_2 = L_1, t) \tag{4}$$

$$G_2 J_2 \frac{\partial \Phi_2}{\partial x_2}(x_2 = L_1 + L_2, t) = T - I_2 \frac{\partial^2 \Phi_2}{\partial t^2}(x_2 = L_1 + L_2, t)$$

with $\Phi_j = \Phi_j(x_j, t)$ being the angular displacement of the column, $\Theta(t)$ an imposed rotation at the top, T the torque-on-bit due to the bit-rock interaction.

3 THE BIT-ROCK INTERACTION MODEL

3.1 The proposed interaction model

Considering the previous work of Richard et al. (2007) as a starting point, an improved bit-rock interaction model is developed. The formulation abandons any assumption limiting backward rotations and bit-bounce.

The dynamics of a blunt cutter are considered, such as the one depicted in Fig. 2. The blunt cutter i has two contact zones where bit-rock interaction exists: $A_{c,i}$, between the rock and the cutting blade; and $A_{f,i}$, between the wearflat and the rock. In this model, the magnitude of the traction vectors (distributed loads) is considered to be constant over each contact region (in the cutter and wearflat, respectively). Its value depends on the following characteristic variables:

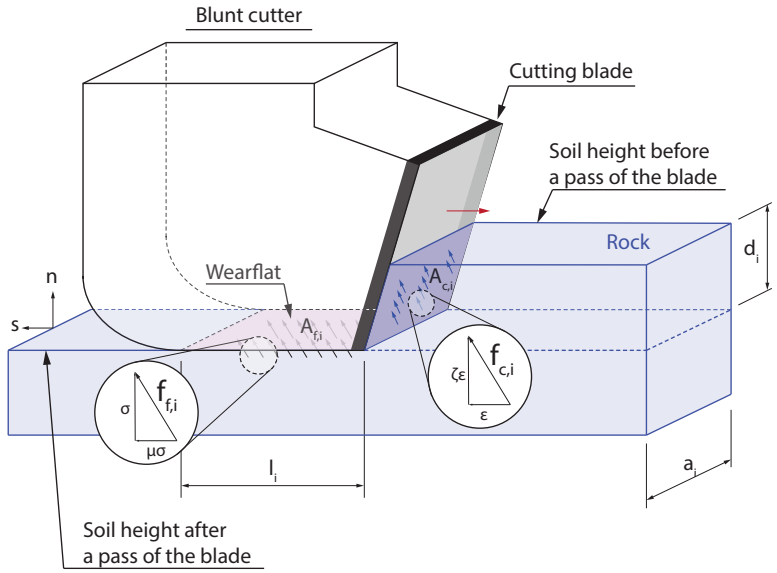

Figure 2: A single cutter i is depicted. The traction vectors $\mathbf{f}_{f,i}$ and $\mathbf{f}_{c,i}$, acting on the wearflat and the cutting blade, respectively, are drawn. These vectors are defined in terms of the function $\sigma(\omega, v)$, that defines the contact pressure at the wearflat, and $\epsilon(\omega)$, an intrinsic specific energy of the rock. The parameter ζ defines the inclination of the cutting force, μ is the coefficient of friction, l_i is the wearflat length, and d_i is the instantaneous depth of cut.

- The rock contact strength function $\sigma = \sigma(\omega, v)$, defined in terms of two contact strength parameters σ_1 and σ_2, and the small regularisation constants c_1 and c_2;
- The rock intrinsic specific energy function $\epsilon = \epsilon(\omega)$, that depends on the intrinsic specific energy parameter ϵ_1 and a regularisation constant c_3;
- the cutter inclination coefficient ζ;
- the coefficient of friction μ.

with ω and v being the torsional and axial speed of the bit. A sketch of the shape of $\sigma(\omega, v)$ and $\epsilon(\omega)$ is depicted in Fig. 3.

If a symmetric and equiangular distribution of blades is considered, and if all the blades have the same associated parameters bit radius $a_i = a$, depth of cut $d_i = d$, wearflat length $l_i = l$, for $i = \{1 \dots n_b\}$, the total force and total torque acting on the bit, considering n_b blades, is

$$\mathbf{W} = \mathbf{W}_c + \mathbf{W}_f, \quad \mathbf{W}_c = \epsilon(\omega)\zeta a d n_b \mathbf{n}, \quad \mathbf{W}_f = \sigma(\omega, v) a l n_b \mathbf{n} \tag{5}$$

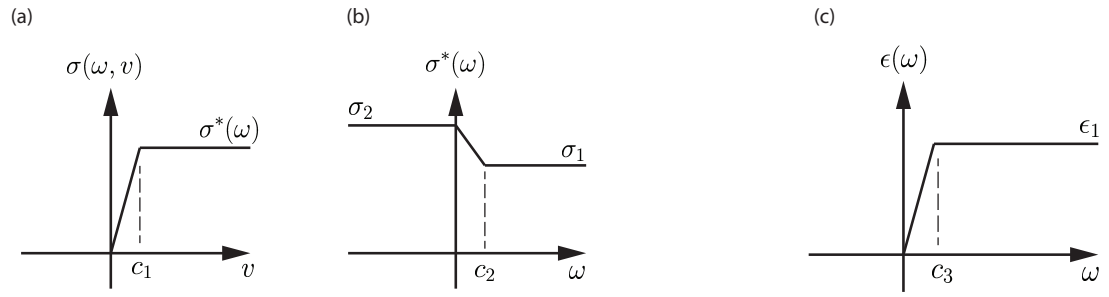

Figure 3: (a) The functional form of $\sigma(\sigma^*(\omega), v)$ is plotted for a fixed value ω; (b) the form of $\sigma^*(\omega)$ is depicted. σ_1 and σ_2 are two parameters associated to the rock contact strength. c_1 and c_2 are some small regularisation constants; and (c) the functional form of $\epsilon(\omega)$ is shown. ϵ_1 is a parameter called the rock intrinsic specific energy and c_3 is some small regularisation constant.

$$\mathbf{T} = \mathbf{T}_c + \mathbf{T}_f, \quad \mathbf{T}_c = \frac{1}{2}\frac{a}{\zeta}\mathbf{W}_c, \quad \mathbf{T}_f = \frac{1}{2}a\mu\gamma\mathbf{W}_f \tag{6}$$

Finally, the previous expressions (5) and (6) require the calculation of d. This is tackled by solving an extra PDE to account for the cutting process, an advection equation.

3.2 Solving the dynamics of the cutting process

The dynamics of the cutting process (the free boundary problem) are obtained by solving the an extra advection equation, as proposed by Wahi and Chatterjee (2008) to simulate the cutting of metals. The main variable $L_s(\eta, t)$ indicates the position of the soil with respect to some reference (zero). The equation takes the form

$$\frac{\partial L_s}{\partial t} + \omega\frac{\partial L_s}{\partial \eta} = 0, \quad \text{with } \eta \in \left[0, \frac{2\pi}{n_b}\right] \tag{7}$$

where n_b is the number of blades. The advection problem is completed with the boundary conditions below.

$$\text{If } \omega \geq 0, \quad L_s(\eta = 0, t) = \begin{cases} U(t), \ L_s(\eta = \dfrac{2\pi}{n_b}, t) < U(t) \\ \\ L_s(\eta = \dfrac{2\pi}{n_b}, t), \ L_s(\eta = \dfrac{2\pi}{n_b}, t) \geq U(t) \end{cases} \tag{8}$$

$$\text{and if } \omega < 0, \quad L_s(\eta = \frac{2\pi}{n_b}, t) = L_s(\eta = 0, t), \tag{9}$$

which means that cutting can only occur if the bit is rotating in the positive direction. In the previous equations, $U(t)$ is the position of the bit.

Finally, at all times the instantaneous depth of cut is given by

$$d_i = \max\left\{L_s\left(\eta = \frac{2\pi}{n_b}, t\right) - L_s\left(\eta = 0, t\right), 0\right\} \tag{10}$$

4 A SPECIAL NON-OSCILLATORY SOLUTION OF THE PREVIOUS EQUATIONS: THE NOMINAL CASE

If a constant angular speed is imposed at the top such that $\Theta(t) = \Omega_0 t$, the formulation employed in models M1 and M2 admits a solution that is non-oscillatory (second time derivatives vanish), for a particular set of initial conditions and boundary conditions, considering a driller operating in the normal cutting regime ($d > 0$, $\omega > 0$, $v > 0$, with $\sigma = \sigma_1$ and $\epsilon = \epsilon_1$) This solution will be referred to as "the nominal case".

Some important constant parameters associated to the nominal solution will be calculated: V_0 (axial speed), T_0 (torque), and d_0 (depth of cut), t_0 (time taken to complete one turn) and t_{n0} (time taken to cover the separation angle between successive blades).

4.1 The nominal case for model M1

The nominal case for model M1 is characterised by the following parameters

$$\Phi_0 = \Omega_0 t - \frac{T_0}{C}, \quad V_0 = \Big(W_0 - \sigma_1 a l n_b\Big)\frac{\Omega_0}{2\pi\epsilon_1 a\zeta} \tag{11}$$

$$d_0 = V_0\, t_{n0} = \frac{V_0 2\pi}{n_b\Omega_0}, \quad \mathbf{T}_0 = \frac{1}{2}\Big(\epsilon_1\, d + \mu\gamma\sigma_1\, l\Big)a^2 n_b\mathbf{n} \tag{12}$$

following the derivation procedure in Richard et al. (2007).

4.2 The nominal case for model M2

The nominal case for model M2 is characterised by the following parameters

$$\Phi_j(x_j, t) = A_j x_j + B_j(t)\ , \quad \text{with } j = \{1, 2\}, \tag{13}$$

$$\text{with } A_1 = -\frac{T_0}{GJ_1}, \quad A_2 = -\frac{T_0}{GJ_2}, \quad B_1 = \Omega_0\, t, \quad B_2 = \frac{J_1 L_1 T_0 - J_2 L_2 T_0 + GJ_2 J_1 \Omega_0\, t}{GJ_2 J_1} \tag{14}$$

where $x_1 \in [0, L_1]$, and $x_2 \in [L_1, L_1 + L_2]$,

$$t_0 = \frac{2\pi}{\Omega_0}, \quad t_{n0} = \frac{2\pi}{n_b\,\Omega_0}, \quad d_0 = \Big(W_0 - \sigma_1 a l n_b\Big)\frac{1}{\epsilon_1 a\zeta n_b} \tag{15}$$

$$V_0 = \frac{d_0}{t_{n0}} = \Big(W_0 - \sigma_1 a l n_b\Big)\frac{\Omega_0}{2\pi\epsilon_1 a\zeta}, \quad \mathbf{T}_0 = \frac{1}{2}\Big(\epsilon_1\, d_0 + \mu\gamma\sigma_1\, l\Big)a^2 n_b\mathbf{n} \tag{16}$$

Finally, the nominal solution for the advection equation (so that d_0 is a constant) is

$$L_s(\eta, t = 0) = -\frac{d_0\, n_b}{2\pi}\eta \tag{17}$$

5 SIMULATION V1: MODEL M1 AS A LIMITING CASE OF M2

It can be shown that model M1 is a particular case of M2 if some hypothesis are introduced. The 2-DOF formulation by Richard et al. (2007) employs a quasi-static approach, what allows the drill-pipes to be represented by a spring with constant C. It also assumes the BHA to be a rigid body. For model M2 to behave like M1, the set of material and geometric parameters need to reflect the previous hypotheses. First, the rigidity of the BHA should be negligible, thus

		Real structure	Model M1	Model M2
Property	Description			
L_1	Drill-pipe length	1000 m	spring (C)	1000 m
L_2	BHA length	200 m	rigid	200 m
N_1	Number of elements (torsion)	-	–	64
N_2	Number of elements (advection)	-	64	64
I, I_2	Lumped inertia	-	$I = 112.67$ kgm^2	$I_2 = (1-\alpha)I$ kgm^2
α	Artificial parameter	-	-	1.00 (*)
C	Rigidity parameter	-	469.05 Nm/rad	-
$\rho, \rho_1,\ \rho_2$	Density	7800 kg/m^3		
r_{po}	Drill-pipe external radius	63.5 mm		
r_{pi}	Drill-pipe internal radius	54.0 mm		
r_{co}	Collar external radius	76.2 mm		
r_{ci}	Collar internal radius	28.0 mm		
$G_1,\ G_2$	Shear modulus	77 GPa		
a	Bit radius	108.0 mm		
l	Drill-bit wearflat length	1.2 mm		
ϵ_1	Rock intrinsic specific energy	0.252 GPa		
σ_1	Rock contact strength	0.252 GPa		
ϵ_2	Rock intrinsic specific energy	0.504 GPa		
σ_2	Rock contact strength	0.504 GPa		
M	Lumped mass	24614.40 kg		
Ω_0	Imposed angular speed	14.42 rad/s		
γ	Drill-bit geometry parameter	1.00		
ζ	Cutter inclination coefficient	0.38		
μ	Coefficient of friction	0.80		
c_1	Regularisation constant	$1 \cdot 10^{-5}$		
c_2	Regularisation constant	$1 \cdot 10^{-1}$		
c_3	Regularisation constant	$1 \cdot 10^{-3}$		

Table 1: List of parameters employed in the simulation. (*) This parameter varies.

$G_2 \to 0$ needs to be considered. Second, an artificial parameter α is introduced so that the propagation speed of the wave equation, given by $v_w = \sqrt{G/(\alpha\rho)}$, can be controlled. In fact, a quasi-static problem is equivalent to considering an infinite propagation speed, compatible with taking $\alpha \to 0$. Additionally, the concentrated inertia, I_2, in the boundary conditions takes the form $I_2 = (1-\alpha)I$. This expression enables the transition from a fully distributed inertia, for $\alpha = 1.00$, to a fully concentrated inertia when $\alpha \to 0$.

The parameters employed in this simulation are shown in Table 1. For simulation V1, the problem is completed with the following initial conditions

$$U(t=0) = 0, \quad \left.\frac{dU}{dt}\right|_{t=0} = V_0, \quad L_s(\eta, t=0) = -\frac{d_0\, n_b}{2\pi}\eta \tag{18}$$

with the following conditions for model M1 only

$$\Phi(t=0) = 0, \quad \left.\frac{d\Phi}{dt}\right|_{t=0} = \Omega_0 + \Delta\Omega_0, \text{with } \Delta\Omega_0 = \Omega_0/10 \tag{19}$$

and the following conditions for model M2 only

$$\Phi_j(x_j, t=0) = 0, \quad \left.\frac{d\Phi_j}{dt}\right|_{t=0} = \Omega_0 + \frac{\Delta\Omega_0\, x_j}{(L_1+L_2)}, \text{with } \Delta\Omega_0 = \Omega_0/10, \tag{20}$$

where V_0 and Ω_0 are constants associated to the nominal solution.

The simulations are calculated using Comsol (COMSOL AB, 2018). The discrete formulation is entered using the ODE equation interface, an the continuous one is introduced in its weak form, in both cases, using Comsol's mathematical module. The advection equation is

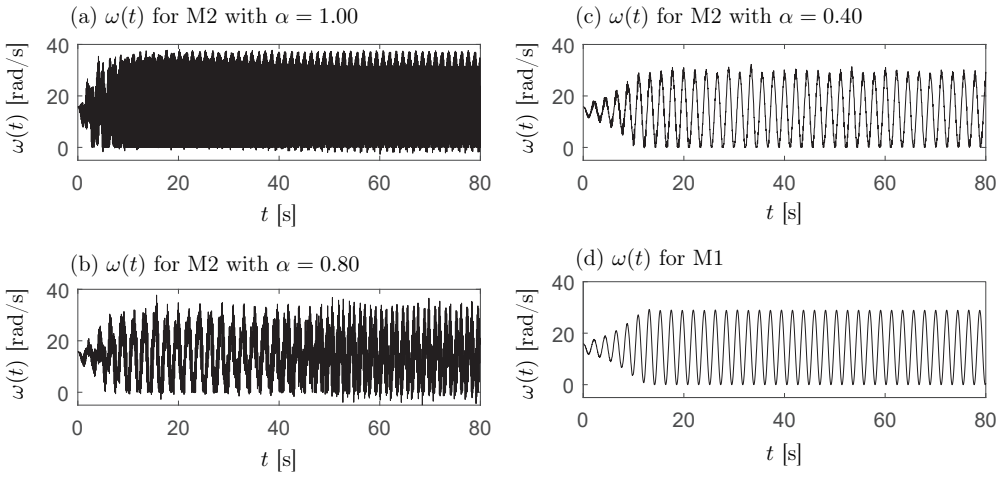

Figure 4: Simulation V2. Angular speed at the bit $\omega(t)$, (a) for model M2 with $\alpha = 1.00$; (b) model M2 with $\alpha = 0.80$; (c) model M2 with $\alpha = 0.40$; (d) Model M1.

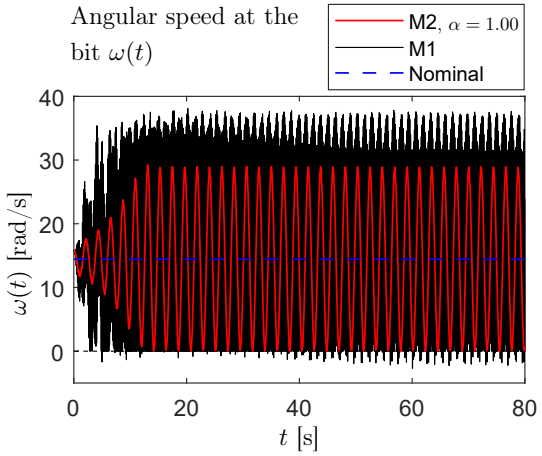

Figure 5: Simulation C1. Angular speed at the bit $\omega(t)$ for the cases C1-A and C1-B (models M1 and M2, respectively). The nominal angular bit speed is shown in dashed line.

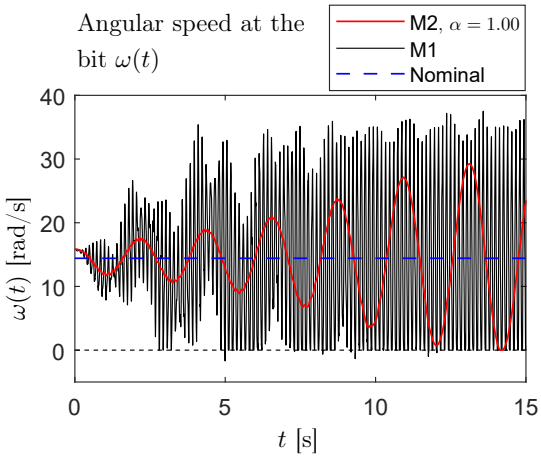

Figure 6: Simulation C1. Angular speed at the bit $\omega(t)$ for the cases C1-A and C1-B (models M1 and M2, respectively). Zoom for $t \in [0\text{s}, 10\text{s}]$. The nominal angular bit speed is shown in dashed line.

already programmed in the built-in transport module. It should be noted that only M2 with $\alpha = 1.00$ has a physical meaning. All smaller values just make s ense in helping to understand how the response varies from a lumped quasi-static formulation with concentrated inertia to a continuous approach. The angular speed at the bit $\omega(t)$ is plotted in Fig. 4 for (a) $\alpha = 1.00$, (b) $\alpha = 0.80$, (c) $\alpha = 0.40$, (d) model M1.

It is observed that, as α evolves from 1.00 in Fig. 4(a) to 0.40 in Fig. 4(c), the simulations become more similar to those of Fig. 4(c) calculated with the 2-DOF model. A graph overlaying the results for M2 with $\alpha = 1.00$ and M1 is shown in Fig. 5, and a zoomed version is shown in Fig. 6. The behaviour changes substantially from one model to another: it is apparent that the frequency content is different.

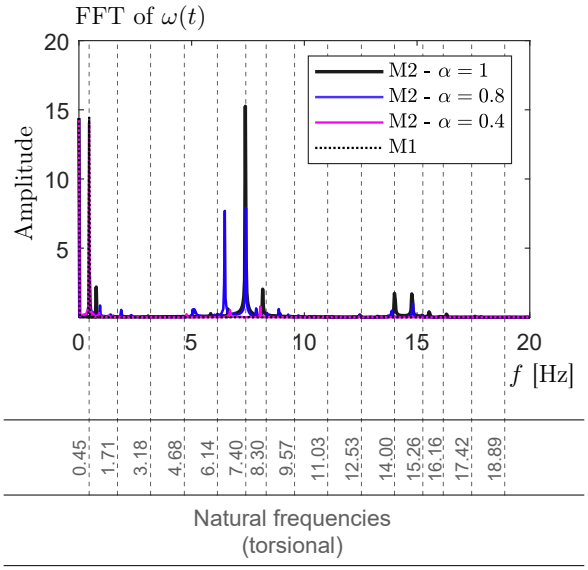

Figure 7: Simulation V2. FFT of the angular speed at the bit $\omega(t)$. Frequency range: 0 to 20Hz.

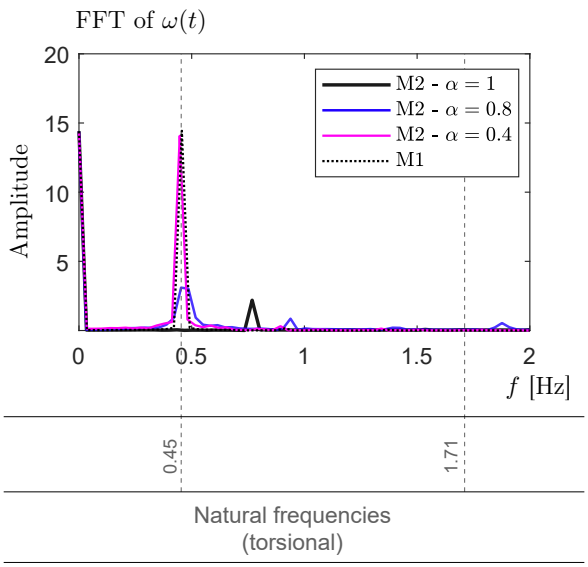

Figure 8: Simulation V2. Zoom of the FFT of the angular speed at the bit $\omega(t)$. Frequency range 0 to 2Hz.

The frequency spectrum of the signal associated to the angular speed is depicted in Figs. 7 and 8, for $t > 50s$, after the transient effects vanish. The results from model M1 contain a main frequency that matches the fundamental one (0.45Hz). This is different for model M2, where the main frequency is close to the sixth natural frequency (7.40Hz), and the amplitudes associated to frequencies close to 0.45Hz are negligible, which explains the appreciable difference observed with the signals in the time-domain.

6 CONCLUSIONS

The first part of this study is an invitation to briefly discuss the use of lumped models and continuous ones for the simulation of drill-string dynamics, as this is not an obvious choice. A comparison of an established 2-DOF model against a continuum approach has been presented. The results herein presented are a first step into exploring the hypothesis that a 2-DOF approach cannot capture the dynamics of a 1200m.

In this study, it is shown that model M1 is a limiting case of M2. The fact that the results do not match, as the frequency spectrum for each signal is very different, means that the hypothesis that lead to model M1 are not being satisfied. Moreover, this is a hint reassuring the original hypothesis that the 2-DOF approach may be inadequate the capture the dynamics of a real-scale drill-string. The results are based on a 1200m-length column, yet the authors expect the discrepancies observed to accentuate even more for a longer driller. It is left for further work to asses the effect of other sources of damping that are not associated to the bit-rock interaction, such as internal structural damping and the effect of the drilling muds.

ACKNOWLEDGEMENTS

This study was financed in part by the Coordenação de Aperfeiçoamento de Pessoal de Nível Superior – Brasil (CAPES) – Finance Code 001; Secretaría General de Ciencia y Tecnología, Universidad Nacional del Sur (Grant No. 24/J075); FONCyT, Agencia Nacional de Promoción Científica y Tecnológica (Grant No. PICT-2015-0220); CONICET (Grant No. 112 201301

00007 CO). The authors would also like to thank the Conselho Nacional de Desenvolvimento Científico e Tecnológico (CNPq) and Fundação de Amparo à Pesquisa do Estado do Rio de Janeiro (FAPERJ) for their financial support.

REFERENCES

Aarsnes U.J.F. and van de Wouw N. Axial and torsional self-excited vibrations of a distributed drill-string. *Journal of Sound and Vibration*, 444:127–151, 2019. ISSN 10958568. doi: 10.1016/j.jsv.2018.12.028.

Brett J.F. The genesis of torsional drillstring vibrations. *Spe Drilling Engineering*, 7(3):168–174, 1992. ISSN 08859744. doi:10.2118/21943-pa.

COMSOL AB. COMSOL Multiphysics® v. 5.4. 2018.

Goicoechea H.E., Buezas F.S., and Rosales M.B. A non-linear Cosserat rod model for drill-string dynamics in arbitrary borehole geometries with contact and friction. *International Journal of Mechanical Sciences*, 157-158(March):98–110, 2019. ISSN 00207403. doi:10.1016/j.ijmecsci.2019.04.023.

Lima R. and Sampaio R. Stick-mode duration of a dry-friction oscillator with an uncertain model. *Journal of Sound and Vibration*, 353:259–271, 2015. ISSN 10958568. doi:10.1016/j.jsv.2015.05.015.

Macdonald K.A. and Bjune J.V. Failure analysis of drillstrings. *Engineering Failure Analysis*, 14(8 SPEC. ISS.):1641–1666, 2007. ISSN 13506307. doi:10.1016/j.engfailanal.2006.11.073.

Piovan M.T. and Sampaio R. Modelos continuos de sondas de perforación para la industria petrolera: Análisis de enfoques y su discretización. *Revista Internacional de Metodos Numericos para Calculo y Diseno en Ingenieria*, 25(3):259–277, 2009. ISSN 02131315.

Richard T., Germay C., and Detournay E. A simplified model to explore the root cause of stick-slip vibrations in drilling systems with drag bits. *Journal of Sound and Vibration*, 305(3):432–456, 2007. ISSN 10958568. doi:10.1016/j.jsv.2007.04.015.

Saldivar B., Mondié S., Niculescu S.I., Mounier H., and Boussaada I. A control oriented guided tour in oilwell drilling vibration modeling. *Annual Reviews in Control*, 42:100–113, 2016. ISSN 13675788. doi:10.1016/j.arcontrol.2016.09.002.

Sampaio R., Piovan M.T., and Venero Lozano G. Coupled axial/torsional vibrations of drill-strings by means of non-linear model. *Mechanics Research Communications*, 34(5-6):497–502, 2007. ISSN 00936413. doi:10.1016/j.mechrescom.2007.03.005.

Tian K. and Detournay E. Influence of PDC bit cutter layout on stick–slip vibrations of deep drilling systems. *Journal of Petroleum Science and Engineering*, 206(February):109005, 2021. ISSN 09204105. doi:10.1016/j.petrol.2021.109005.

Trindade M.A., Wolter C., and Sampaio R. Karhunen-Loève decomposition of coupled axial/bending vibrations of beams subject to impacts. *Journal of Sound and Vibration*, 279(3-5):1015–1036, 2005. ISSN 0022460X. doi:10.1016/j.jsv.2003.11.057.

Vaisberg O., Vincké O., Perrin G., Sarda J.P., and Faÿ J.B. Fatigue des tiges de forage: État de l'art. *Oil and Gas Science and Technology*, 57(1):7–37, 2002. ISSN 12944475. doi:10.2516/ogst:2002002.

Wahi P. and Chatterjee A. Self-interrupted regenerative metal cutting in turning. *International Journal of Non-Linear Mechanics*, 43(2):111–123, 2008. ISSN 00207462. doi:10.1016/j.ijnonlinmec.2007.10.010.